Polymers **2014**, *6*, 820-845; doi:10.3390/polym6030820

OPEN ACCESS

polymers

ISSN 2073-4360

www.mdpi.com/journal/polymers

Article

Morphologies and Thermal Variability of Patterned Polymer Films with Poly(styrene-*co*-maleic anhydride)

Pieter Samyn [1,*] and Gustaaf Schoukens [2]

[1] Chair for Bio-based Materials Engineering, Faculty for Environment and Natural Resources, University of Freiburg, Werthmannstrasse 6, 79085 Freiburg, Germany

[2] Department of Textiles, Ghent University, Technologiepark 907, 9052 Zwijnaarde, Belgium; E-Mail: gustaaf.schoukens@ugent.be

* Author to whom correspondence should be addressed; E-Mail: pieter.samyn@fobawi.uni-freiburg.de; Tel.: +49-761-203-9239; Fax: +49-761-203-3673.

Received: 20 January 2014; in revised form: 28 February 2014 / Accepted: 3 March 2014 / Published: 14 March 2014

Abstract: Patterned films of poly(styrene-*co*-maleic anhydride) copolymers were deposited by dip-coating from acetone solutions. A qualitative study of the film morphologies shows the formation of polymer spheres with smaller diameters at higher amounts of maleic anhydride (MA), and long-fibrous features at higher molecular weights. Upon heating, the films progressively re-assemble with short- and long-fibrous structures as a function of heating time and temperature. In parallel, the film morphologies are quantified by image processing and filtering techniques. The differential scanning calorimetry confirms the higher glass transition temperatures with increasing amount of MA. The analysis with Raman spectroscopy shows interactions between the molecules in solution and effects of ring-opening (hydrolysis) and ring-closure (formation of MA) during drying of the films. The water contact angles on the patterned films are within the hydrophilic range. They mainly correlate with the amount of MA moieties calculated from spectroscopy, while the roughness parameters have a minor effect. The variations in film patterns illustrate the self-assemble ability of the copolymers and confirm a heterogeneous molecular structure, as previously assumed.

Keywords: copolymer; film; pattern; spherical; fibrous; heating; wetting

1. Introduction

The creation of thin patterned films with soft materials is a flexible and versatile method for surface modification. Polymer films are likely prepared by spin-coating or dip-coating and classified as ultrathin films with a thickness < 100 nm or thin films with a thickness of 100 to 10,000 nm [1]. Due to the (visco-)elasticity of polymer films, the morphology can be influenced by interactions with the substrate or by external effects such as, e.g., temperature [2], humidity [3], pressure [4], electricity [5], light [6] or direct convection [7]. The adaptable morphology and response to external stimuli provides an excellent way for *in situ* handling of the morphology and properties of the polymer film. From a practical point of view, polymers films are likely applied in membranes, sensors, coatings, or general surface functionalization in material and life sciences. The ordered polymer films can be further used as templates for nanopatterning [8]. From a more fundamental point of view, a study on film morphologies and thermal stability brings additional insight in the physical mechanisms for polymer arrangement and the chemical polymer structure.

Structured polymer films can be assembled through physical mechanisms driven by mechanical stress [9], capillary forces [10], dispersion forces [11] or crystallization [12]. Otherwise, the polymer chain assembly relies on the chemical and electronic interactions between a monolayer and a substrate [13], or a combination of inter- and intramolecular interactions, which might be influenced by effects such as molecular recognition, charge separation, electron transfer and/or hydrophilic and hydrophobic forces within or between adjacent polymer chains [14]. Traditionally, patterned polymer films are obtained by the controlled phase separation on surfaces with regions of different surface tension [15,16], or by the arrangement of sequences in block copolymers [17]. The formation of surface patterns from spin-cast films is caused by a solvent quench, in which the solvent is removed rapidly from the polymer solution and induces phase separation of the two dissolved polymers. The segregation of the components in a polymer blend is largely controlled by the surface energy, and it has been demonstrated that the component with the lower surface free energy is generally enriched at the air-polymer surface [18]. The most fundamental insights in film patterning result from the understanding of the dewetting mechanisms of thin polymer films [19] and phase separation [20]. For thin polystyrene films, the correlated dewetting could explain the appearance of satellite holes and their positions relative to pre-existing holes [21]. The dewetting properties of polystyrene films could be inhibited by adding poly(methyl methacrylate), which stabilizes the film for certain concentrations and molecular weights [22]. Another method for patterning of a polymer film includes the addition of a doping agent, which might result in buckling of the polymer film. Otherwise, the spontaneous buckling of specific polymer components also results in film patterning [23,24]. After deposition of a maleic anhydride (MA) film onto a solid surface, the film morphology is most likely in a metastable phase that is influenced by surface constraints or specific film components [25], and it may undergo various morphological transitions towards a thermodynamic equilibrium with annealing [26]. The heating above the glass transition temperature leads to destabilization of the film: in the early stages of dewetting holes are formed due to thermal fluctuations (spinodal dewetting) [27] or a nucleation and growth process starting at defects [28]; in the last stage of dewetting a regular (spinodal dewetting) or an irregular (nucleation and growth process) structure is formed. The thermal instabilities of polystyrene diblock copolymers are related to the microphase separation temperature: for a moderate

annealing of surface-deposited films, an exponentially decaying lamellar order of alternating copolymer segments is observed with annealing time [29], while aggressive annealing of a free-standing polystyrene film leads to the formation of holes [30].

The molecular self-assembly of polymer systems provides a powerful tool to form micro- to nanoscale patterned films from ternary systems (polymer/polymer blends = two polymers in a common solvent), block copolymers [31], and homopolymers [32]. The ordering in supported thin films of symmetric and asymmetric AB diblock and ABA triblock copolymers was recently reviewed, along with that of more complex materials such as ABC triblocks and liquid crystalline block copolymers [33]. General surface patterns observed in block copolymer and homopolymer films include honeycomb structures, stripes and random polymer aggregates on the surface: e.g., polystyrene/poly-paraphenylene [34], or polystyrene/b-oligothiophenes and aromatic amide dendrons [35] mainly form hexagonal honeycomb structures. The amphiphilic character of polystyrene block copolymers plays a crucial role as a surfactant, while a monodisperse pore size is obtained when star-polymers or micelles are used. The honeycomb micropatterns are often formed by so-called breath figures [36] and could be further optimized by close control of parameters such as polymer concentration, humidity, casting area and solvent [37]. As studied by ToF-SIMS, the formation of film patterns through self-organization is directly related to the role of polar terminations [38]. The structures can finally be further stabilized after crosslinking and serve as a self-supported three-dimensional structure [39]. Otherwise, the poly-styrene/polymethacrylate diblock [40], polystyrene/polybutadiene triblock [41] or polystyrene/poly-isoprene [42] copolymers form cylindrical microstructures. The phase behavior of the copolymer can be modeled by a dynamic density functional theory, and the stability region for each surface pattern depends on an interplay between surface fields and confinement effects.

Poly(styrene-co-maleic anhydride) or styrene maleic anhydride (SMA) copolymers have gained interest as a functional polymer due to the reactivity of the MA groups in the backbone. The low-molecular weight polymers are typically synthesized by a radical polymerization and have an alternating molecular structure with narrow polydispersity of the molecular weight distribution (M_w/M_n = 1.04). The surface patterns of spin-cast films with formation of honeycomb holes have been extensively studied and are explained as traces of water droplets emulsified by the hydrolyzed SMA [43–45]. As such, the patterned SMA films were used to support the organization of nanoparticles into Langmuir-Blodgett films [46]. The glass transition of poly (styrene-*co*-MA) cumene-terminated films was determined by a mechanical relaxation experiment [47], while the morphology of the polymer monolayer depends on the presence of electrolyte in the water subphase [48]. The thermal annealing of MA copolymers likely causes a reorientation of the polymer chains that improve the mechanical anti-wear properties [49]. On the other hand, the high-molecular weight SMA copolymers have a more heterogeneous molecular structure, with alternating copolymer segments containing high and low amounts of styrene and MA, statistically distributed over the copolymer chain [50]: in summary, the SMA copolymers show a trend with increasing fractions of alternating and decreasing fractions of semi-/non-alternating structures as the nominal amount of MA increases. While the composition with a nominal amount of 50 mol % MA has a fully alternating molecular structure, the alternating domains are separated by semi- or non-alternating domains as the nominal amount of MA decreases. This specific molecular structure allows for conversion of SMA into spherical nanoparticles during imidization [51].

As the latter nanoparticle formation failed in reactions with low-molecular SMA, we further focus on the intrinsic molecular characteristics of the SMA copolymers.

From previous overview, the heterogeneous molecular structure of the high-molecular weight SMA copolymers can result in the formation of patterned polymer films. In this work, we provide additional evidence for the assembly of high-molecular weight SMA leading to film patterns with either spherical or fibrous morphology, in parallel with their thermal stability and wetting properties.

2. Experimental Section

2.1. Materials

Styrene maleic anhydride (SMA) copolymers with different molecular weights (M_w = 80,000 to 180,000 g/mol) and amounts of maleic anhydride (MA = 22 to 34 mol %) were obtained from Polyscope (Geleen, The Netherlands) as pellets. The properties of six different SMA grades used in this study were previously determined by chromatography and NMR and are summarized in Table 1 [50]. The polydispersity of the SMA copolymers ranges between 2.35 and 2.73 and is within characteristic values for free radical copolymerization.

Acetone (Sigma-Aldrich, Diegem, Belgium) was used as a solvent for film formation. Stock solutions of SMA were prepared by dissolving 10 mg/mL SMA in acetone (pH = 7) and magnetically stirring for 1 h at 23 °C. When necessary, the stock solutions were further diluted for additional characterization.

Table 1. Characterization of different grades of styrene maleic anhydride (SMA).

SMA grade	M_n [g/mol]	M_w [g/mol]	M_z [g/mol]	M_w/M_n	Amount maleic anhydride (MA) [mol %]
SMA-1	35185	80000	181000	2.28	26
SMA-2	54620	120000	260000	2.21	26
SMA-3	65640	180000	328000	2.76	26
SMA-4	47050	110000	257000	2.35	22
SMA-5	41000	110000	236000	2.73	28
SMA-6	31100	80000	150200	2.59	34

2.2. Film formation

Thin films of SMA copolymers were deposited onto microscope glass slides that were rinsed with acetone and D.I. water. The slides were vertically dip-coated into the stock solutions of SMA in acetone (10 mg/mL), while applying a controlled withdrawal speed of 5 mm/min that was experimen-tally chosen to yield most homogeneous films (in contrast to higher withdrawal speeds resulting in inhomogeneous films according to preliminary tests). After evaporation of the acetone, the films were dried for one day under controlled air (23 °C, 50% relative humidity). The films were subsequently heated in a circulating hot-air oven for 1 to 10 h at temperatures of 120, 150, 180, 200 and 250 °C. The films with highest thermal stability were supplementary heated for 5 h at 280, 300 and 320 °C.

2.3. Characterization Methods

The SMA copolymers were characterized by differential scanning calorimetry (DSC) under continuous nitrogen flow by loading 5.0 ± 0.1 mg of the pulverized sample into an aluminum pan (Q2000 equipment, TA Instruments V3.9A, Zellik, Belgium). Two heating cycles were applied, with a fixed heating and cooling rate of 10 °C/min in the temperature range of 0 to 250 °C and an isothermal period of 5 min at the highest and lowest temperatures. Before testing, the DSC was calibrated with indium (melting point 156.6 °C, ΔH = 28.45 J/g) and gallium (melting point 29.8 °C).

The structural conformations and stability of SMA in acetone solutions were further characterized by size measurements (on 1 mg/mL solution) and zetapotential measurements (on 10 mg/mL solution) at 25 °C, using a standard He-Ne laser of 633 nm, 3 mW (Zetasizer ZS-90, Malvern Instruments, Worcestershire, UK). For size measurements, the non-invasive backscatter technology (NIBS) with 90° scattering angle is applied on diluted solutions of 1 mg/mL SMA, which allows to detect sizes of 0.3 nm to 5 µm (diameters). The data was analyzed by Malvern's software (v 6.01, Malvern Instruments, Worcestershire, UK), using a Multiple Narrow Modes (non-negative least squares, NNLS) algorithm for calculating the multimodal size distributions weighted by intensity. For zetapotential measurements, electrophoretic light scattering is applied on the stock solutions (10 mg/mL). In parallel, viscosity measurements were performed on the stock solutions (10 mg/mL) at 25 °C, using a Brookfield viscometer (Brookfield Ltd., Lorch, Germany) at 20 rpm. The Fourier-transform Raman (FT-Raman) spectra of acetone solutions and films were recorded on a Spectrum GX equipment (Perking Elmer, Rodgau, Germany). The spectra were averaged over 64 scans with a Nd:YAG laser power of 500 mW at a resolution of 4 cm^{-1} between 100 and 3400 cm^{-1}.

The morphology of SMA films was studied by optical microscopy, using an BX51 microscope (Olympus, Hamburg, Germany). The microscopic images were further analyzed with Image J 1.47 software in order to obtain qualitative morphological data. By using selected image filters (explained and illustrated in the Results Section), a histogram of specific film features could be made. The films were also evaluated by tapping-mode atomic force microscopy (AFM), using a PicoScan 2500 PicoSPM II Controller (PicoPlus, Molecular Imaging, Tempe, AZ, USA) with silicon probe (k = 40 N/m, resonant frequency 300 kHz). All films morphologies were evaluated under ambient air conditions (23 ± 2 °C; 50% ± 5% relative humidity).

Contact angles of D.I. water were measured on SMA films, using a Digidrop equipment (GBX, Bourg-de-Peage, France). For static contact angle measurements, a fixed volume of water was placed on the surface films (6 µL), or for dynamic contact angle measurements the droplet volume was gradually increased to a maximum of 6 µL (advancing contact angle) and afterwards the volume was reduced (receding contact angle) in contact with the surface film. The droplets were fitted with Laplace–Young (static) and tangent (dynamic) procedures.

3. Results and Discussion

3.1. Fundamental Thermal and Spectroscopic Analysis

In order to examine the heating sensitivity of the films more accurately in the following sections, the thermal characteristics of SMA copolymers were first evaluated by DSC measurements. The

thermographs for various SMA grades with different amount of MA (*i.e.*, SMA-1, -4, -5, -6) and different molecular weight (*i.e.*, SMA-1, -2, -3) are shown in Figure 1, representing the glass transition interval in the second heating cycle. A summary of the glass transition temperatures T_g together with onset and end temperatures of the transition interval is given in Table 2. The temperature T_g mainly depends on the amount of MA and increases from 147.5 to 175.8 °C with higher amount of MA (22 to 34 mol %) in the order of SMA-4, -1, -5, -6. Otherwise, the temperature T_g is less dependent on the molecular weight (80,000 to 180,000 g/mol) and remains constant at around 158.34 ± 0.15 °C by comparing SMA-1, -2, -3. In parallel, the SMA-1 that was dissolved in acetone and dried as a free-standing film has a slightly higher T_g = 159.74 ± 0.20 °C than the bulk SMA-1. Similar trends were observed for other SMA grades, with a maximum T_g = 178.15 ± 0.25 °C for a SMA-6 cast film. In general, solvents could lead to plasticization or residual amounts retained in the polymer film after casting, both lowering T_g [52]. However, the slight augmentation of T_g after solvent casting rather suggests a constraint mobility of chain segments in the amorphous phase caused by additional interactions [53]. The differences in T_g for dried films can be explained on the basis of the thermodynamic polymer chain interactions in solution, *i.e.*, the physical properties of a solution-cast polymer film may be affected by the conformation of the polymer chain in the solvent. The thermo-analytical data confirm that the SMA molecules likely interact in the solvent and form self-assembled structures that are transferred into the dried film.

Figure 1. DSC curves for SMA copolymers, indicating the glass transition temperatures T_g, (**a**) different SMA grades in pulverized pellet form; and (**b**) SMA-1 grade in pulverized pellet form and as acetone film after air drying.

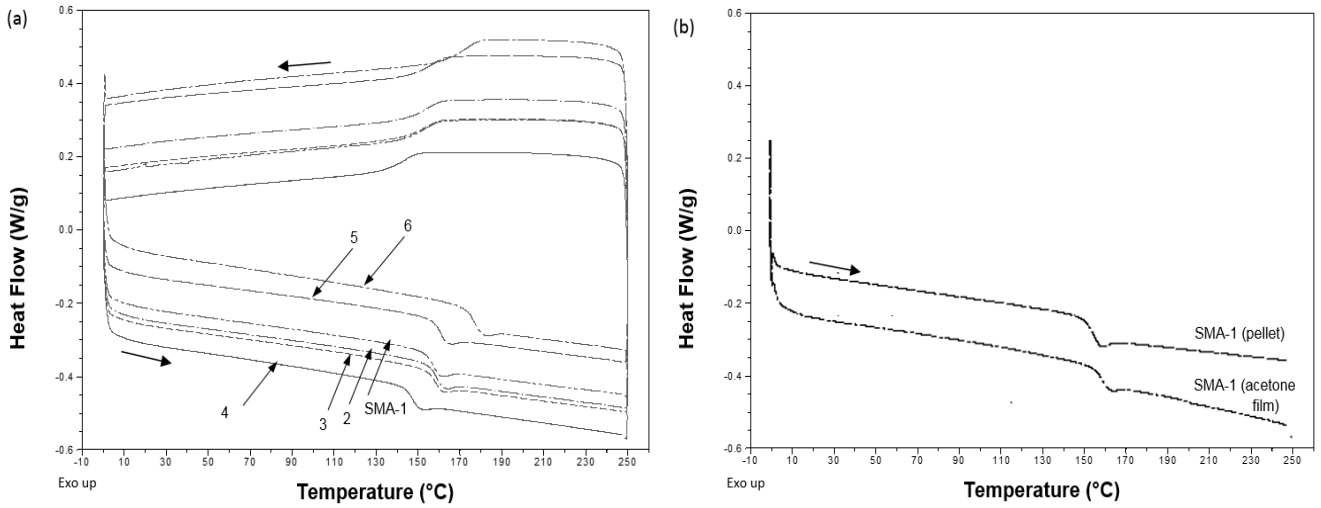

The FT-Raman spectra of SMA copolymers were first measured in an acetone solution as shown in Figure 2, e.g., for SMA-1 with concentrations of 5 and 10 mg/mL. Compared with the spectra of pure acetone, there is an upwards shift in the peak positions from 786.8 to 788.8 cm^{-1} and a downwards shift in the peak positions from 1710.1 to 1706.8 cm^{-1} for the SMA/acetone solutions (see insets Figure 2). The variations in band positions indicate that the interactions between the polymer and the solvent are located near the C–H (788 cm^{-1}, stretching of acetone) and C=O (1710 cm^{-1}, stretching mode) functional groups of the SMA [54] and the acetone [55]: the molecules of acetone and SMA can

aggregate to form dimers with hydrogen bonds around C=O (1710 cm^{-1}), between the oxygen atom of one molecule and the hydrogen atoms of a CH/CH_3-group of another molecule. The variations in C–H stretching bands of the acetone (788 cm^{-1}) likely relate to the occurrence of acetone solvating molecules around the SMA.

Table 2. Summary of data from DSC curves of different SMA grades: characteristic temperatures for the glass transition interval.

SMA grade	T_{onset} [°C]	T_g [°C]	T_{end} [°C]	ΔT [°C]
SMA-1	153.43	158.19	159.20	5.77
SMA-2	155.02	158.32	160.12	5.10
SMA-3	154.59	158.52	159.35	4.76
SMA-4	144.08	147.53	148.81	4.73
SMA-5	156.74	160.34	161.87	5.13
SMA-6	172.30	175.81	178.85	6.55

Figure 2. Raman spectra of stock solutions of SMA-1 in acetone solvent used for film casting, (**i**) pure acetone; (**ii**) acetone + SMA (5 mg/mL), (**iii**) acetone + SMA (10 mg/mL); and (**iv**) SMA pellets.

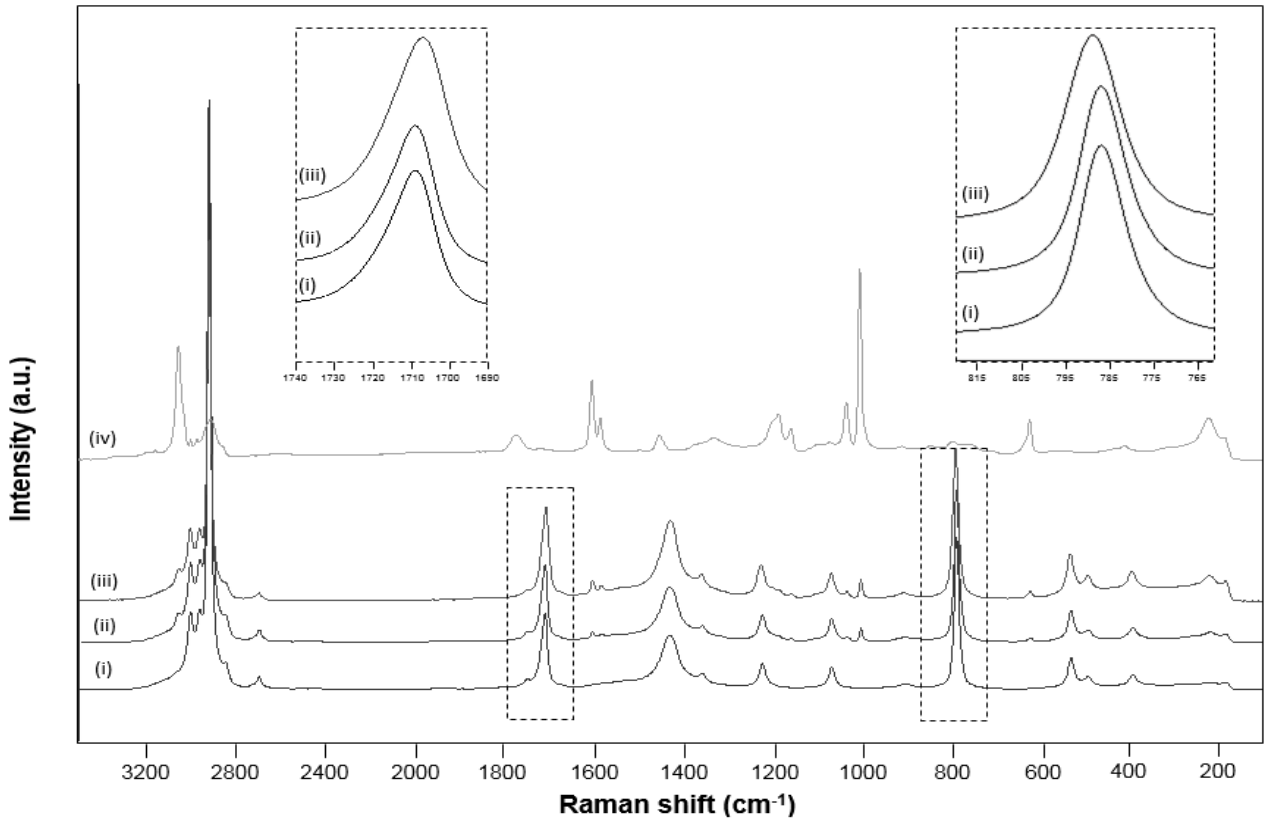

After casting a film from acetone solution and heating for 1 h at 120 °C, the Raman spectra were evaluated again as illustrated in Figure 3. It can be concluded that the films do not contain residual solvent as the absorption peaks of acetone disappeared from the Raman spectra. After one day air-drying, the spectra of SMA films and pellets are different: the lower intensity of the 1857 cm^{-1} band for the

acetone film indicates that the anhydride groups in the SMA films have been partly converted by a ring-opening reaction, forming carboxylic groups. These ring-opened groups might induce additional molecular interactions as also expressed by the small intensities of additional Raman bands at 667 and 366 cm^{-1}. After heating the film, the spectra of the films become similar to the original SMA pellets. The ring-opened anhydride moieties are restored after heating of the acetone-cast films at temperatures above 120 °C. The above analysis was repeated for several SMA grades, and all observations lead to likewise conclusions.

Figure 3. Raman spectra of SMA-1 films cast from acetone solution, (**i**) initial SMA pellets; (**ii**) SMA-1 film cast from acetone after one day air-drying; and (**iii**) SMA-1 film cast from acetone after heating for 1 h at 120 °C. Arrows refer to variations described in text.

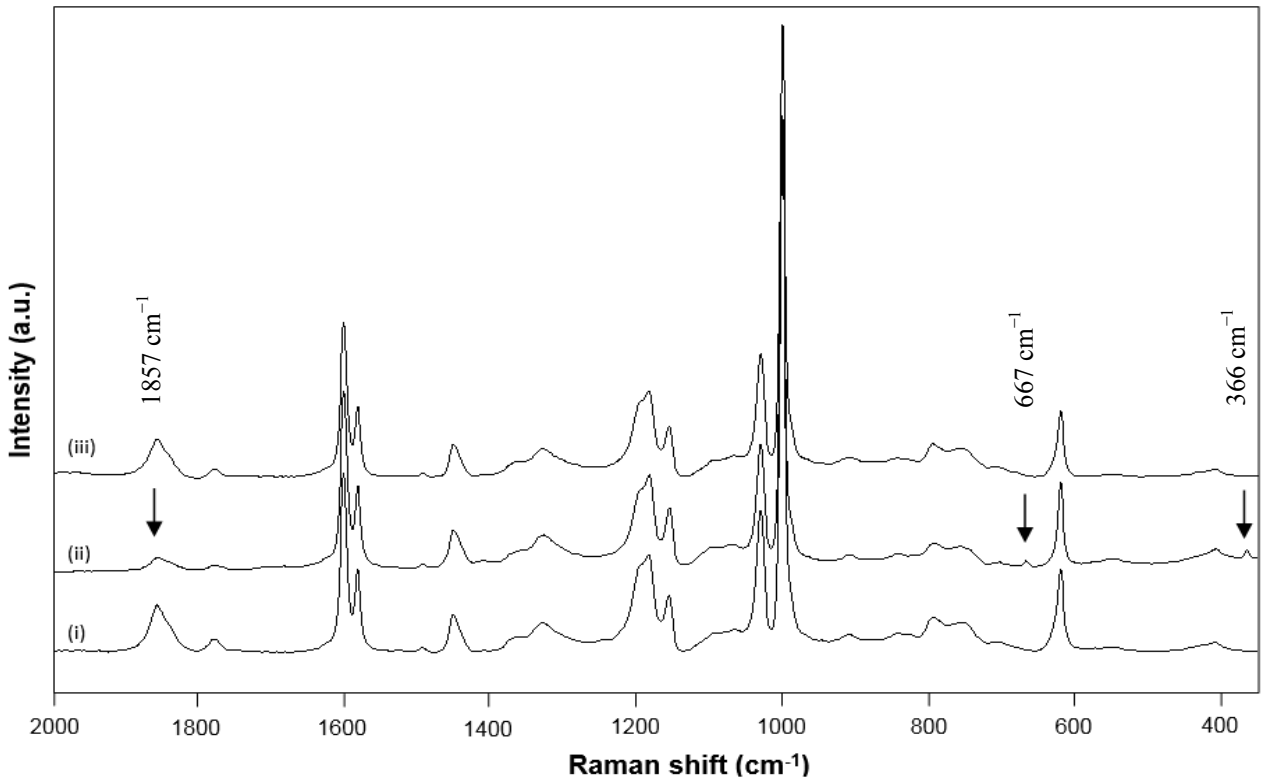

3.2. Characteristics of the Acetone Solutions

The acetone solutions of SMA copolymer grades turned opaque, as an indication that assembled molecular structures might be formed. Therefore, the acetone solutions were further characterized by size and zetapotential measurements. An example of the intensity size distributions for SMA-1 and SMA-6 solutions is illustrated in Figure 4, averaged from 400 (100 measurements × 4 runs) scans per sample. The measurements were taken after short-time sonication of the solution and show the presence of micro- and nanoscale structures. These curves only confirm the existence of the aggregates, but no further conclusion on their relative amount can be made. Based on the presence of the peaks, there exists a microscale fraction with diameters of 3.8 μm (SMA-5), 2.6 μm (SMA-1), 1.3 μm (SMA-5) and 0.8 μm (SMA-6). As a general trend, the diameters of the microscale aggregates reduce at higher amount of MA by comparing the SMA-4, -1, -5, -6. Otherwise, the diameter slightly

increases at higher molecular weight by comparing the SMA-1, -2, -3. According to the previously detailed heterogeneous molecular structure of SMA [50], organized molecular structures likely form through self-assembly of the styrene parts (hydrophobic) and maleic anhydride parts (hydrophilic).

Figure 4. Intensity size distribution of dissolved SMA in acetone, measured with Zetasizer ZS-90, e.g., for SMA-1 (26 mol % MA) and SMA-6 (34 mol % MA) demonstrating broad distribution of sizes with microscale aggregates.

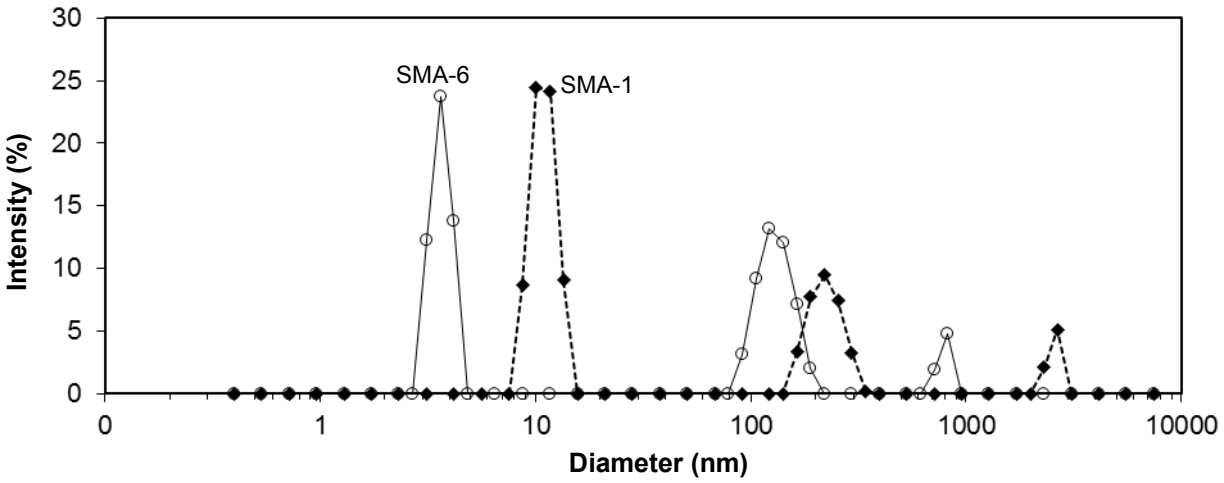

In parallel, the zetapotential values in Table 3 ($\zeta = -50$ to -60 mV) are a result of dissociation of the maleic anhydride moieties into carboxylic groups providing negative charges. From viscosity measurements, a slight increase in viscosity with amount of MA and molecular weight of the SMA copolymers is noticed. This provides further evidence for molecular interactions and assembly of the molecules in solution: as the amount of MA increases, electrostatic interactions around the maleic anhydride moieties (or partially converted into carboxylic groups) are expected to increase due to the larger number of dissociated groups; as the molecular weight increases, polymer chains may likely be more entangled (at least at high concentrations $c >> c^*$) and have more interaction sites per molecule. Both phenomena may lead to an increase in viscosity of the solution. The consequent formation of structured films on glass substrates as discussed below, shows that the assembled structures were transferred from solution into a surface-deposited patterned film.

Table 3. Physical characteristics of acetone solutions for different SMA grades.

SMA grade	Zetapotential [mV]	Viscosity [cps]
SMA-1	−57 ± 1	58 ± 2
SMA-2	−56 ± 1	98 ± 2
SMA-3	−58 ± 1	103 ± 5
SMA-4	−50 ± 1	50 ± 3
SMA-5	−60 ± 1	68 ± 2
SMA-6	−62 ± 1	72 ± 3

3.3. Film Morphology Depending on SMA Grade

Films of SMA copolymer grades were formed by dip-coating glass slides in an acetone solution and evaporation of the solvent during one day under air conditions (23 °C, 50% RH). The deposition resulted in patterned films with different morphologies depending on the SMA grade, as described below.

First, the influence of amounts of MA on the film morphology was investigated by comparing the films of SMA-4, -1, -6 with optical microscopy and AFM height images as shown in Figure 5. The films cover the glass substrates homogeneously with polymer spheres. The spherical diameters *d* are largest for SMA-4 (Figure 5a, MA = 22 mol %: *d* = 4 to 5 µm), and they become systematically smaller for SMA-1 (Figure 5b, MA = 26 mol %: *d* = 1.5 to 2 µm), and SMA-6 (Figure 5c, MA = 34 mol %: *d* = 1 to 1.5 µm). It is concluded that the spherical diameter gradually decreases at higher content of MA. For different SMA grades, the spherical diameters were quantified from five independent microscopic photographs with twenty readings of the diameters. Based on these readings, a histogram of the spherical diameter distribution is presented in Figure 5d. Although there is an overlap in the size-distributions of the spheres for different SMA grades, the spherical diameter with maximum frequency decreases gradually with amount of MA. There is a trend that the width of the size distribution becomes more narrow (and the spherical diameters more homogeneous) at higher amounts of MA.

Figure 5. Film morphology of SMA copolymer grades with different percentages of maleic anhydride, by optical microscopy and AFM height images: (**a**) SMA-4; (**b**) SMA-1; (**c**) SMA-6; and (**d**) histogram of spherical diameters for different SMA copolymer grades.

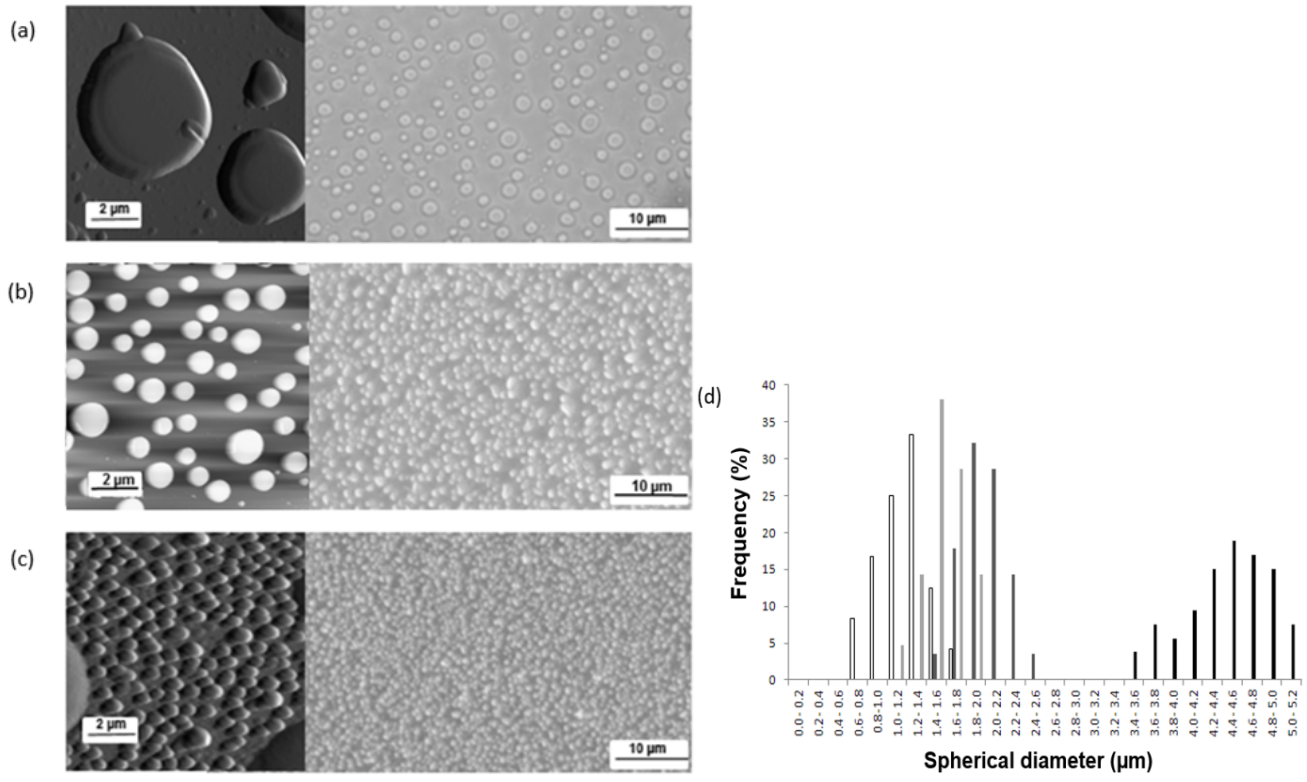

Second, the influence of molecular weight on the film morphology was investigated for the films of SMA-1, -2, -3 as shown in Figure 6. For SMA copolymers with the same amount of MA

(MA = 26 mol %), structured thin films have formed with spherical morphology for SMA-1 (M_w = 80,000 g/mol, Figure 6a), a mixed morphology of spheres and fibers for SMA-2 (M_w = 120,000 g/mol, Figure 6b) and a fibrous morphology for SMA-3 (M_w = 180,000 g/mol, Figure 6c). The spheres have a relatively uniform shape, with heights in the range of 500 nm and diameters in the range of 1 μm. The fibers have a diameter of 1 μm and consist of entangled fibrils with elementary diameters of about 300 nm diameters. From these observations, the fibrous structures are formed above a critical molecular weight at which the assembly into spheres becomes unlikely.

Figure 6. Film morphology of SMA copolymer grades with different molecular weight, by optical microscopy and AFM height images: **(a)** SMA-1; **(b)** SMA-2; and **(c)** SMA-3.

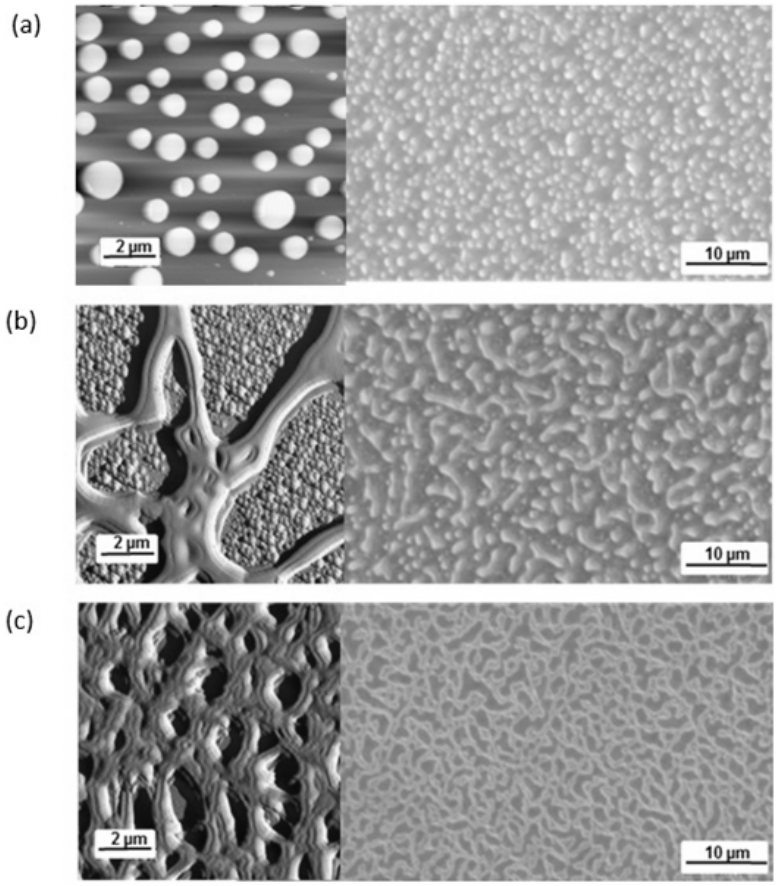

3.4. Film Morphology Depending on Thermal Heating

The thermal stability of the patterned films and morphological transitions were further studied after heating at different temperatures and times in a hot-air oven. The thermal morphology changes can provide fundamental information on the tendency for molecular assembly of SMA copolymers, and have practical implications for using them as thermo-sensitive films with variable wetting properties.

In a first series of tests, the influence of heating temperatures between 100 and 250 °C was investigated for a constant heating time of 5 h. A global overview on the films of SMA-1, after deposition and after heating for 5 h at 250 °C is shown in Figure 7, illustrating good macroscopic homogeneity over the entire glass substrate without tendency for macroscopic dewetting. The film morphologies and changes in local morphology of the spherical structures are further detailed in

Figure 8 during stepwise heating at various temperatures, indicating good stability. The polymer spheres retain their shape up to temperatures of 180 °C and partly deform into larger aggregates at 200 and 250 °C. This is expressed by a broadening of the distribution curves for spherical diameters at higher temperatures, as shown in Figure 9. However, still a significant amount of spheres (about 50%) remains thermally stable in the original form above the temperature T_g = 158 °C. The latter can be due to either interface effects by chemical attachment of the particles to the surface and/or thermodynamically-driven effects. It is remarkable that the particles do not merge into a continuous film and the effects of the molecular assembly remain existing at higher temperatures. The morphologies for films of SMA-4 and SMA-6 copolymers are detailed in Figure 10 under the same heating conditions of 5 h at 120, 150 or 250 °C. After heating, the film pattern for SMA-4 (T_g = 147 °C) is instable above 120 °C, while the film pattern for SMA-6 (T_g = 176 °C) is completely stable for all heating temperatures. This might be expected from the low T_g temperature for SMA-4 and the high T_g temperature for SMA-6, although the applied heating temperature of 120 °C is still far below the temperature T_g for SMA-4 and 250 °C is far above the temperature T_g for SMA-6. The higher amount of MA in SMA-6 likely contributes to stronger inter- and intramolecular chain interactions providing thermal stability. The most stable films of SMA-6 had finally to be heated for 5 h up to 280 °C before any variation in the film morphology with a rearrangement of the polymer spheres occurred, as shown in Figure 11. After heating for 5 h at 320 °C, the film starts to re-assemble with alignment of the spheres that do not merge together.

Figure 7. Microscopic overview of patterned films for SMA-1 copolymer, **(a)** after deposition; and **(b)** after heating for 5 h at 250 °C.

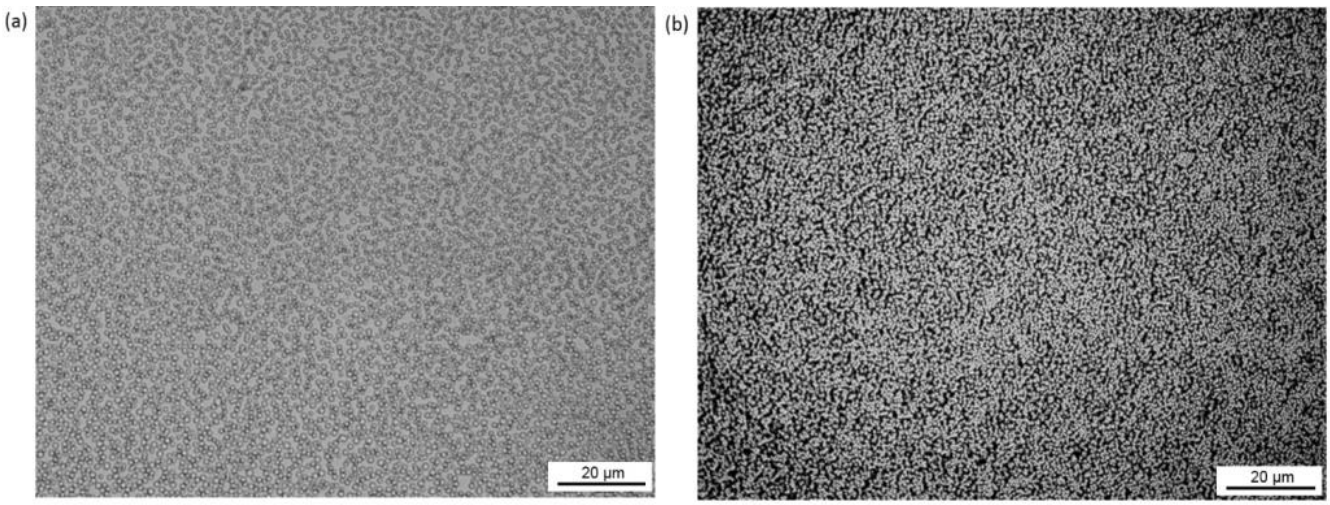

Figure 8. Detailed microscopic evaluation of patterned films for SMA-1 after heating for 5 h at different temperatures, (**a**) 120 °C; (**b**) 150 °C; (**c**) 180 °C; (**d**) 200 °C; and (**e**) 250 °C.

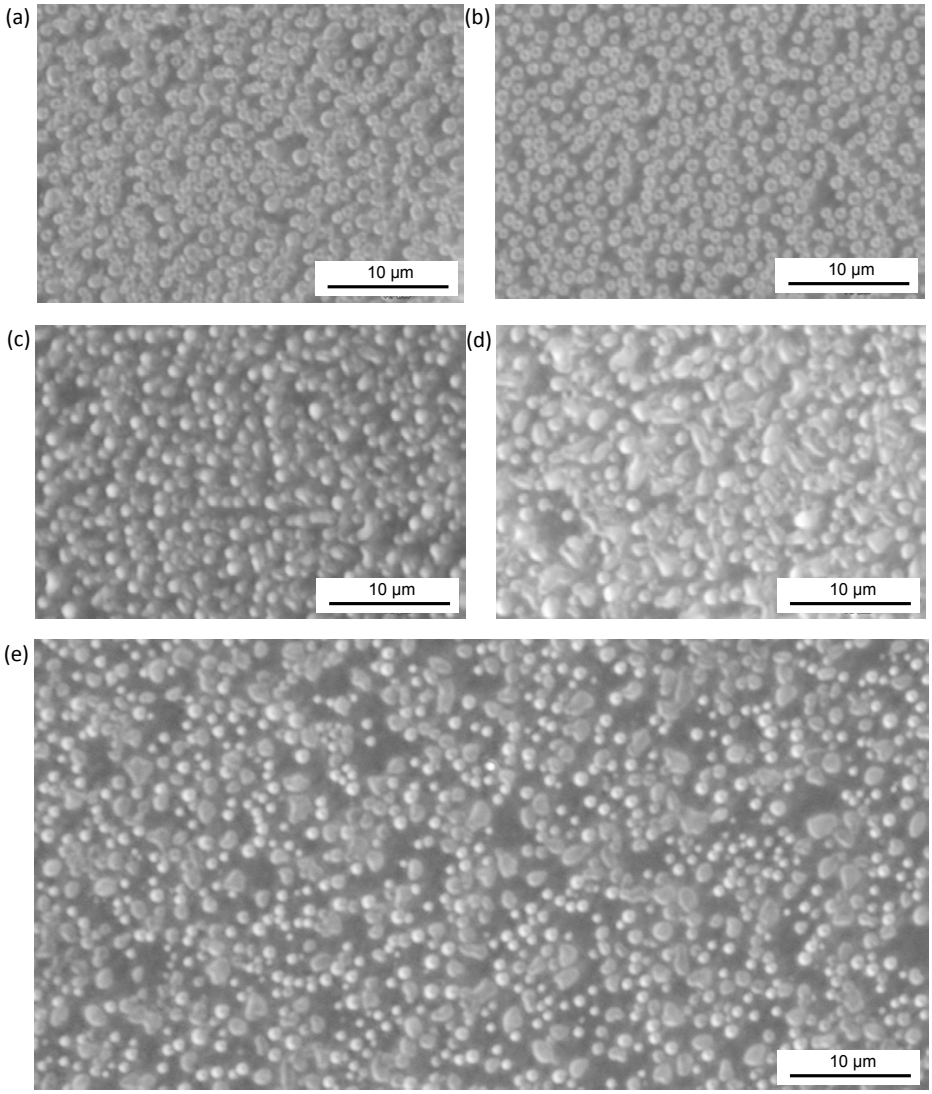

Figure 9. Detailed microscopic evaluation of patterned films for SMA-1 after heating for 5 h at different temperatures, (**a**) 120 °C; (**b**) 150 °C; (**c**) 180 °C; (**d**) 200 °C; and (**e**) 250 °C.

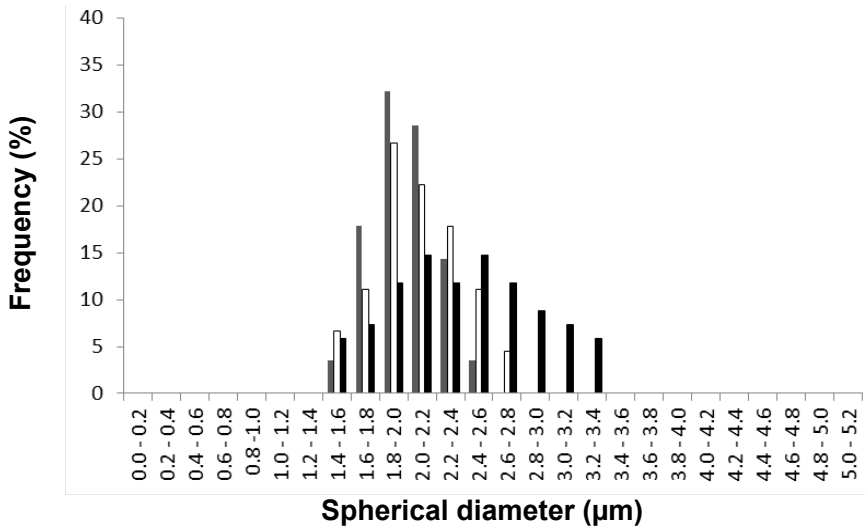

Figure 10. Detailed microscopic evaluation of patterned films for other SMA grades after heating for 5 h at different temperatures, (**a**) SMA-4 at 120 °C; (**b**) SMA-4 at 150 °C; (**c**) SMA-6 at 180 °C; and (**d**) SMA-6 at 250 °C.

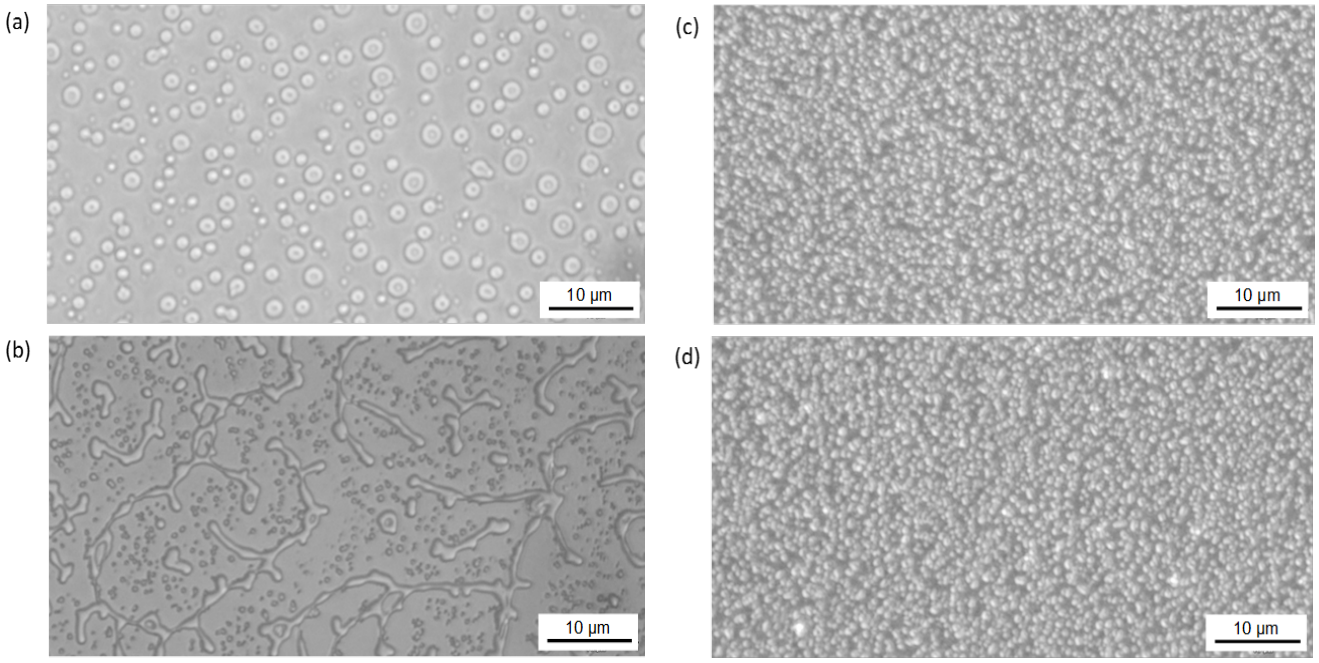

Figure 11. Detailed microscopic evaluation of patterned films for SMA-6 after heating for 5 h at different temperatures, (**a**) 280 °C; (**b**) 300 °C; and (**c**) 320 °C.

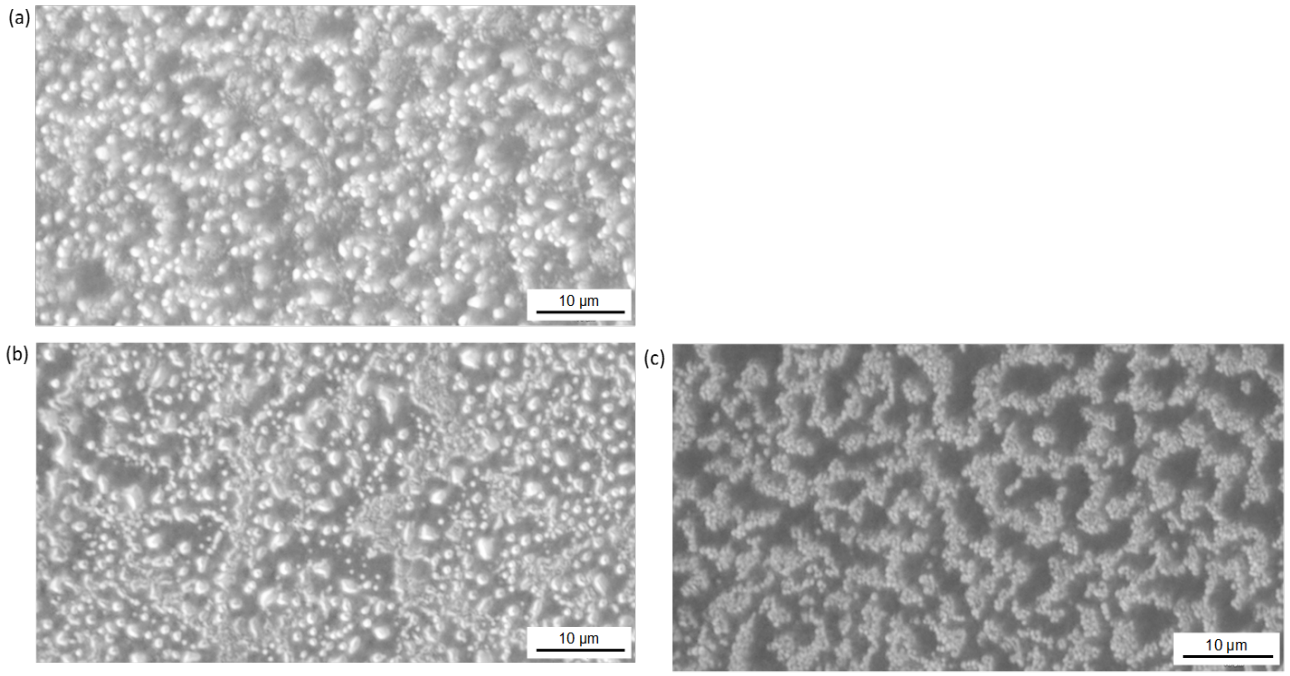

In a second series of tests, the influence of heating time near the glass transition temperature of the SMA copolymer was evaluated. The morphology changes in films of copolymers with lowest glass transition temperature were first investigated (SMA-4: T_g = 147 °C). After heating for short times of 1 to 3 h at 150 °C, a progressive re-assembly of the polymer spheres over the surface with gradual

lining-up over the surface was observed, as shown in Figure 12. The re-arrangements finally result in a network structure as shown before after 5 h heating (Figure 10b). The films of copolymers with higher glass transition temperature (SMA-1: T_g = 158 °C) and good thermal stability after 5 h heating at 150 °C (see before, Figure 8b) were subsequently heated for 10 h. An interesting variation in film morphology is noticed with a transformation of the spherical structures into a fibrous network over longer time, as shown in Figure 13. This drastic morphological change indicates that the film is mobile and can move over the surface.

Figure 12. Detailed microscopic evaluation of patterned films for SMA-H4 after heating at 150 °C for different times, (**a**) 1 h; (**b**) 2 h; and (**c**) 3 h (5 h similar to Figure 10b).

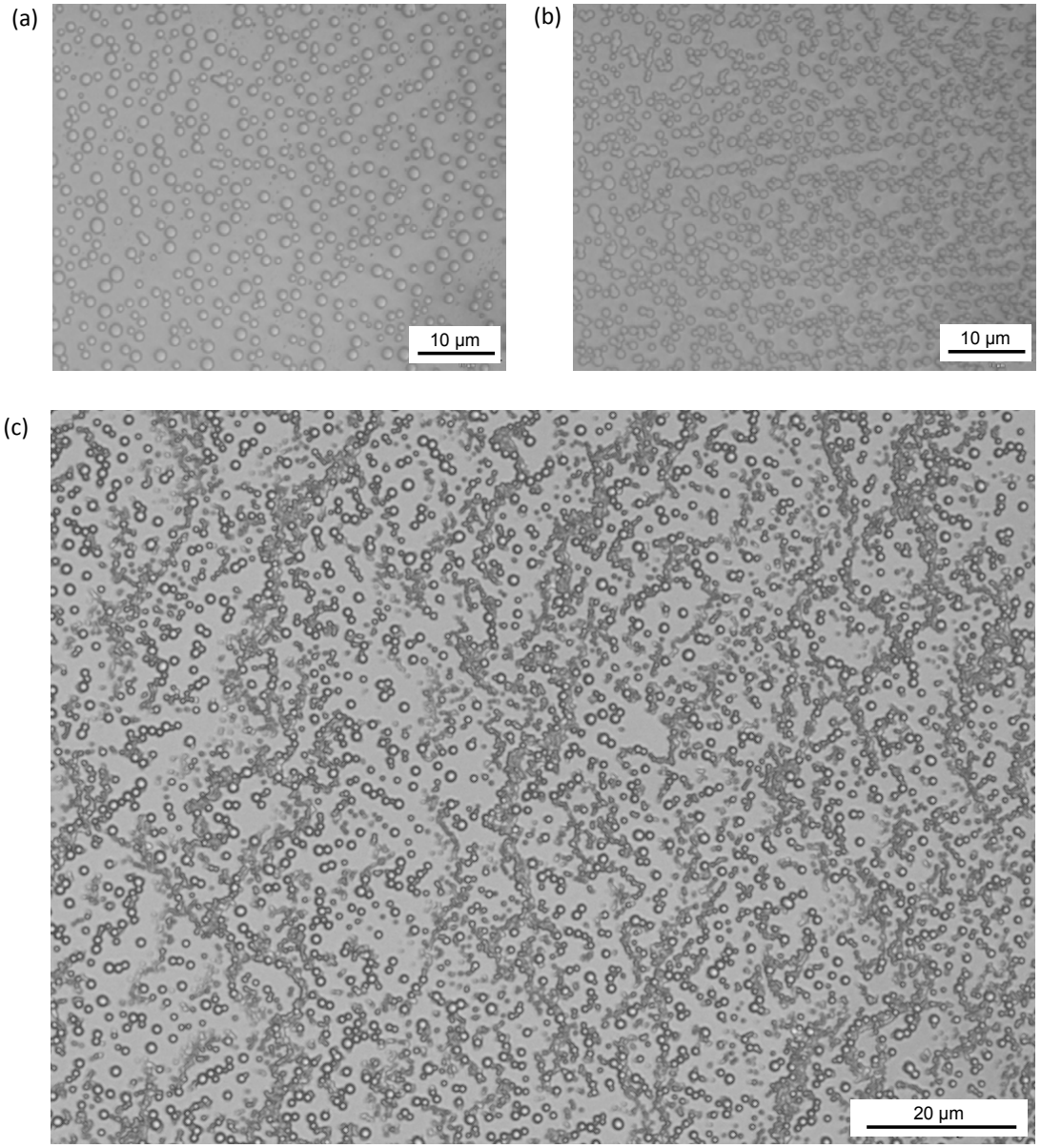

The formation of a thermally stable fibrous network structure was also noticed for films of copolymers with a higher molecular weight, *i.e.* SMA-2 (M_w = 120,000 g/mol) and SMA-3 (M_w = 180,000 g/mol), immediately after deposition of the film and without heating (Figure 14). The formation of a fibrous network can likely be related to the high viscosity of the solutions with high

molecular weight copolymers (*i.e.*, compare SMA-1, -2, -3). The fibrous structure remained stable during heating, as an indication that this is a more stable structure over a broad range of molecular weight and temperatures. In comparison with the fibrous structures formed after heating of SMA-1 copolymers (M_w = 80,000 g/mol), however, the structures of high-molecular weights SMA-2 and SMA-3 are somewhat thicker. From these morphologies, it can be concluded that the assembly into spheres is metastable and develops at intermediate molecular weights (SMA-1, -4, -5, -6: M_w = 80,000 to 110,000 g/mol) and in a certain temperature interval. A detailed picture of the stabilized fibrous films of SMA-1 upon heating for several hours at temperatures below the glass transition temperatures is shown in Figure 15a (optical microscopy) and in Figure 15b (AFM). The film thickness is about 200 to 300 nm, according to a 2D profile generated from the AFM images in Figure 15c. Here, the diameter of the fibers can be estimated, and from similar graphs for other SMA copolymers we observe an increase in diameters for SMA copolymers with different molecular weight as follows: 1.5 to 2 µm for SMA-1, 2 to 2.5 µm for SMA-2, and 3 to 4 µm for SMA-3. Moreover, the fibers are composed by a parallel assembly of single fibrils. The diameter of the single fibrils (about 400–500 nm) remained almost constant for all SMA copolymers, while a larger amount of fibrils was lining-up as the SMA copolymer contains higher amount of MA. Some specific features during thermal heating of the SMA copolymer films are highlighted in Figure 16, indicating local re-arrangements in the film morphologies (e.g., for SMA-1). Both AFM images at scanning sizes 10 × 10 µm^2 (Figures 16a,c) illustrate the progressive agglomeration of polymer spheres upon heating for 5 h at 200 and 250 °C, respectively. More interesting features are included in the pictures at scanning sizes of 2 × 2 µm^2 (Figures 16b,d): here, the formation of smaller spherical capsule sizes over the surface is observed: the latter suggests that the film dewets over the surface and the remaining film in the dewetting areas re-assemble into elementary particle sizes of around 100 nm at the final thermal heating temperature of 250 °C for 5 h.

Figure 13. Detailed microscopic evaluation of patterned films for SMA-1 after heating at 150°C for different times, (**a**) 7 h; (**b**) 8 h; (**c**) 9 h; and (**d**) 10 h.

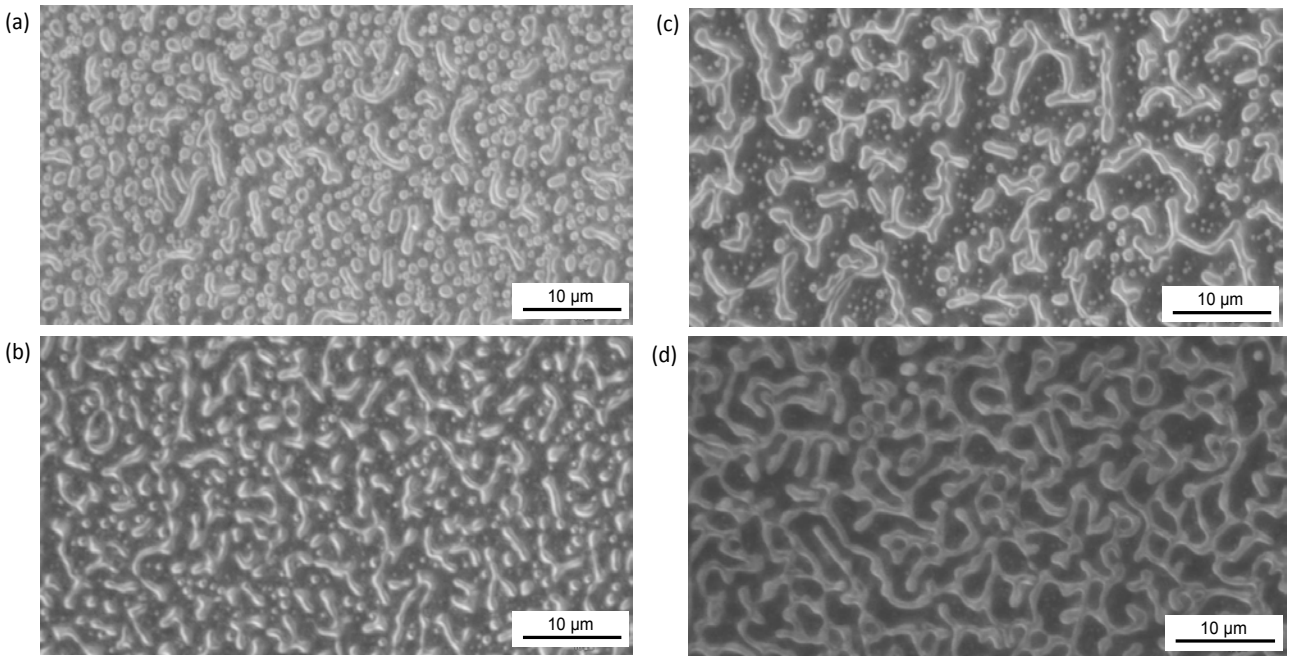

Figure 14. Detailed microscopic evaluation of patterned films for SMA copolymers with different molecular weight, immediately after depositions and no heating: (**a**) SMA-2 (M_w = 120,000 g/mol); and (**b**) SMA-3 (M_w = 180,000 g/mol).

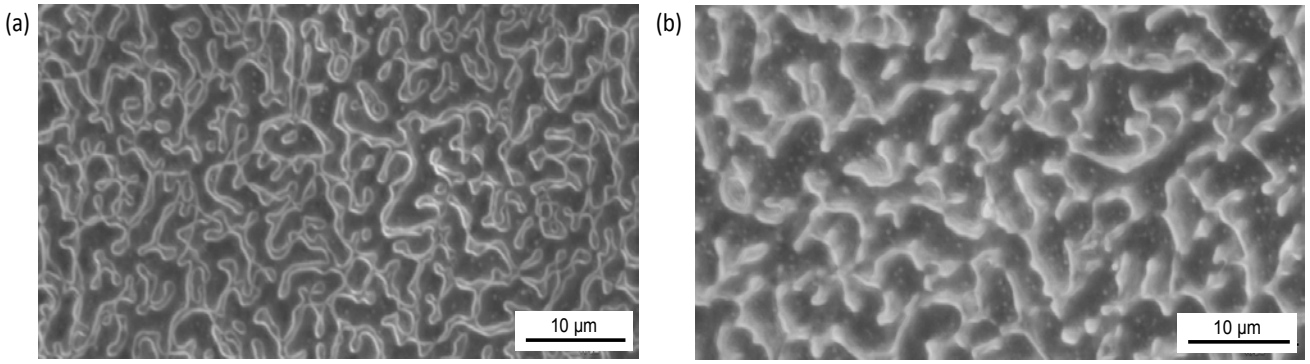

Figure 15. Stabilized fibrous film pattern of SMA-1 after thermal curing for 10 h at 150 °C, **(a)** detail by optical microscopy; **(b)** AFM height image; and **(c)** profile from AFM.

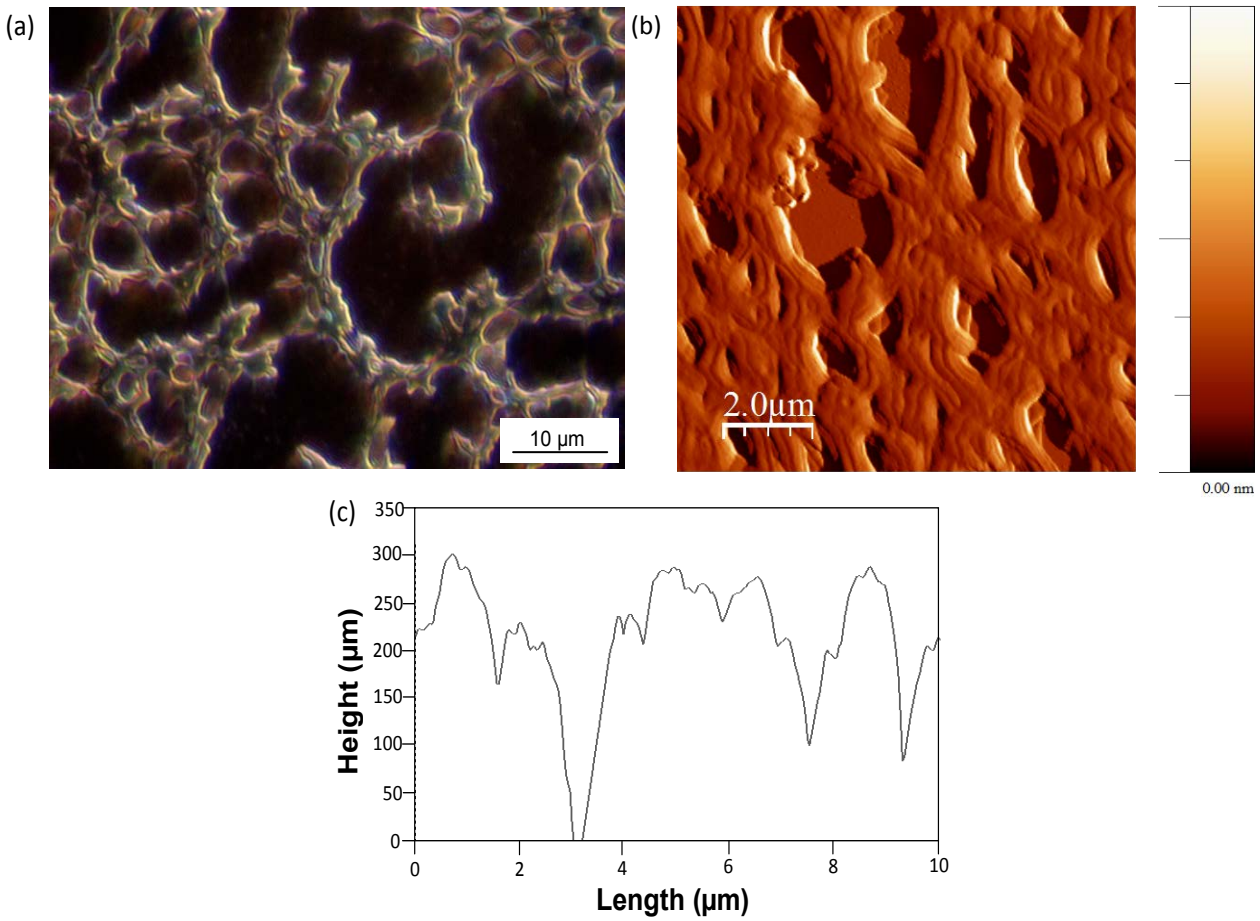

Figure 16. AFM images of specific features on films with SMA-1 copolymer after thermal curing, (**a**,**b**) SMA-1 (5 h at 200 °C); (**c**,**d**) SMA-1 (5 h at 250 °C). Circles in images (**a**) and (**c**) indicate the positions where magnifications (**c**) and (**d**) were taken. Left legend applies for (**a**,**c**) and right legend applies for (**b**,**d**).

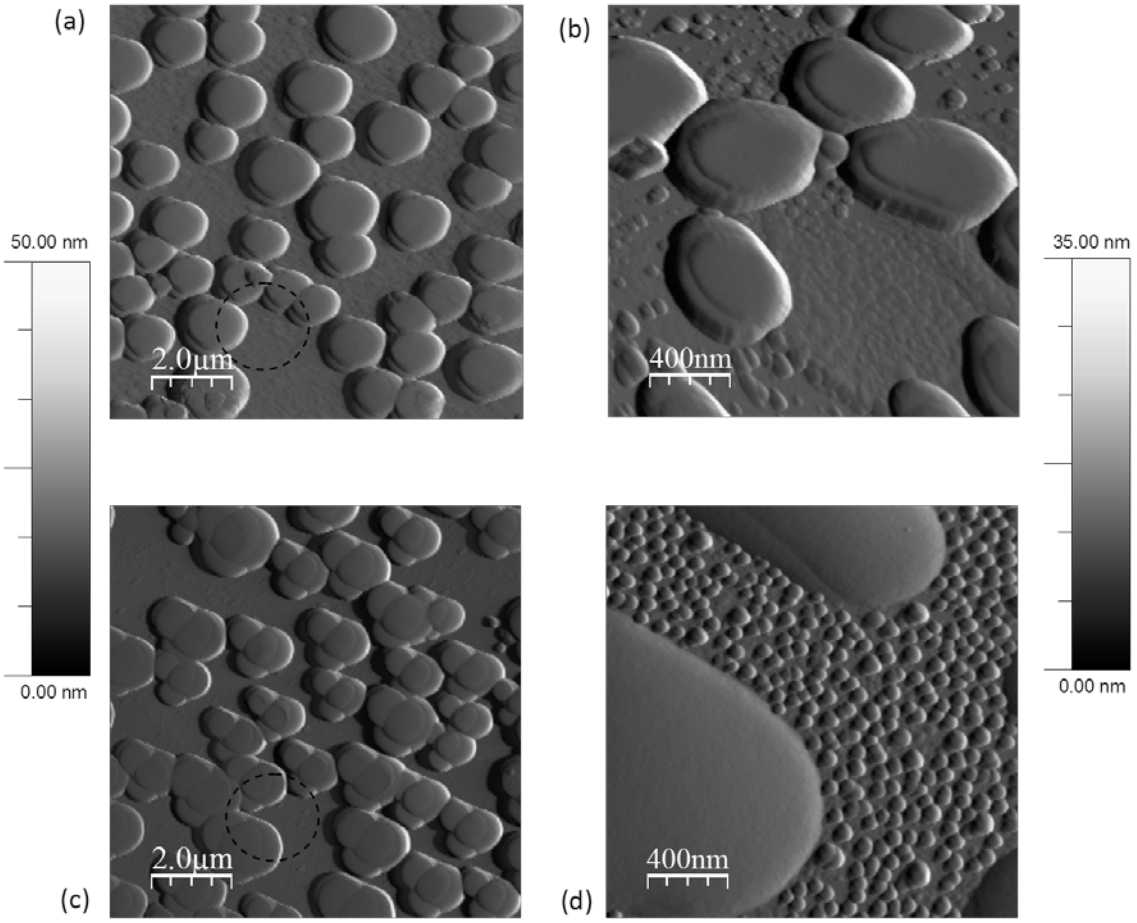

3.5. Quantitative Morphologies

The gradual transformation from spherical into fibrous structures during heating was further quantified by image processing of the optical micrographs, determining the contributions of various film morphologies.

The images were first transformed into 8-bit images and the edges of the film structures were automatically determined by the image software. An illustration of the original and processed images is shown in Supplementary Information and Figures S1–S6. In order to quantify the amount of each feature, the surface coverage (area) for each image object category was determined, which is related to the number of white pixels in a black-and-white processed image. Therefore, the spheres were determined as structures with a given maximum diameter of 2 µm. The short-fibrous structures were a priori determined as structures with a given threshold value for surface coverage, corresponding to structures with length between 1 and 5 µm. The fibrous network structures were determined as structures with a surface coverage above the threshold value. In order to make a histogram of the surface features, two different filters were used to subsequently remove the specific elements from the image. Standard mathematical procedures for image filtering were used, including a spherical filter

element with increasing diameter to filter the spherical shapes and an elliptical filter with increasing size to filter the fibrous structures (an example of filtered images in subsequent steps is shown in Supplementary Information and Figures S1–S6). As such, the all of the image objects are step by step removed from the image.

The percentages of spherical, short-fibrous and continuous fibrous network structures were determined, e.g., for SMA-1 and SMA-6, after heating at different temperatures up to 10 h (Figure 17). The histograms quantify the progressive transformation of a spherical into fibrous morphology at heating times up to 10 h. It confirms the progressive formation of almost completely long-fibrous structures (up to 90%) for SMA-1 at 150 to 200 °C, and the formation of mainly short-fibrous structures (up to 90%) and a small fraction long-fibrous structures (up to 8%) for SMA-6 at 150 to 200 °C. The shape of the histograms directly reflects the lower thermal stability of film patterns for SMA-1 and high thermal stability of film patterns for SMA-6.

Figure 17. Quantitative image analysis of film morphologies for SMA-1 and SMA-6 after thermal heating at different temperatures and times, representing spherical (first column), short fibrous (second column) and long fibrous structures (third column) for (**a**) SMA-1 at 150 °C; (**b**) SMA-6 at 150 °C; (**c**) SMA-1 at 200 °C; and **(d)** SMA-6 at 200 °C.

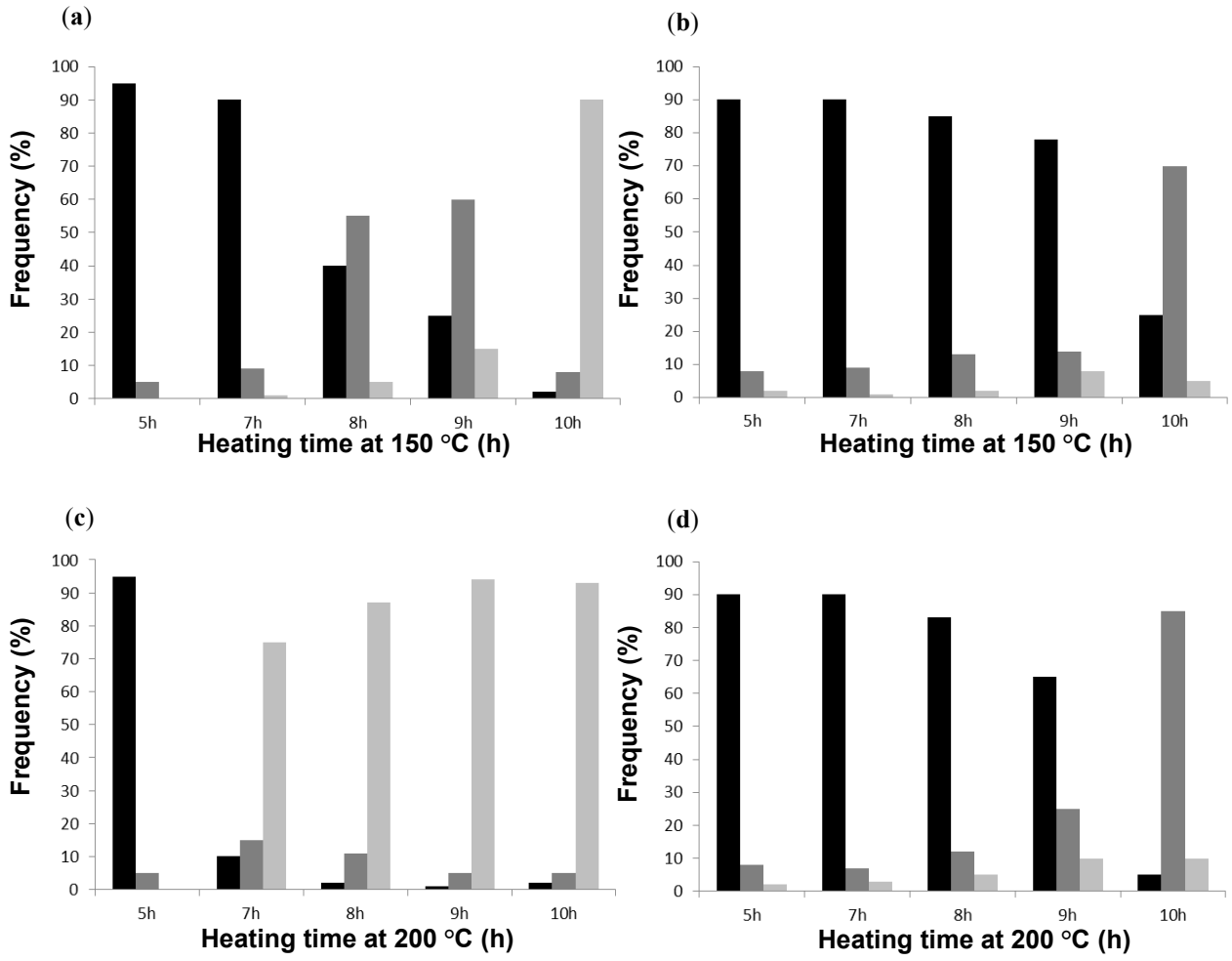

3.6. Contact Angle Measurements

The water contact angles on SMA copolymer films with various amounts of MA and heating temperatures (5 h) are summarized in Table 4. The standard deviation on static contact angles θ_{stat} was about ±2.1°, according to three repetitive measurements per polymer film. A reference value for static water contact angles on uncoated glass substrate is θ_{stat} = 48° ± 1.1°. The standard deviation in dynamic advancing contact angles θ_a is somewhat larger and about ±3.5°, with a reference value on uncoated glass substrates of θ_a = 52° ± 1.8°.

The contact angles for SMA copolymer films vary with the amount of MA and thermal heating, but are all in the hydrophilic range. For the non-heated films, θ_{stat} are between 62° to 50° and decrease in the order SMA-4, -1, -5, -6: it can be concluded that the higher amount of MA implies higher hydrophilicity to the polymer film, as the MA groups are more hydrophilic than the styrene parts. Otherwise, the effect of thermal heating is relatively reproducible for all SMA grades, with a first trend of slight decrease in contact angle at low heating temperatures (100 °C), followed by a second trend in increasing contact angles at higher heating temperatures (120 °C) and finally a stabilization and slight decrease in contact angles at the highest temperatures (150 to 250 °C). According to previous characterization of SMA films with Raman spectroscopy, the variations in contact angles upon heating may reflect the influences of film hydrolysis (open-ring structure of the MA groups) and reformation of the MA (closed-ring structure). The dynamic advancing contact angles θ_a are very near to the static contact angles in case of SMA-4, while some more significant differences are measured for SMA-6. Mainly, the variations in dynamic contact angles with higher amount of MA are not as clear as the variations in static contact angles, because the dynamic contact angles are more sensitive to the combination of surface chemistry and topography. The receding contact angles θ_r on the SMA copolymer films are not explicitly mentioned, as these values were almost <20 °C in all cases.

In general, wetting of the polymer films is expected to depend on the chemical composition and surface topography. Therefore, the amount of MA (from Raman measurements, Figure 3) and average surface roughness R_a (from AFM measurements, Figure 5) were determined and are given in Table 5. The amount of MA was calculated as the intensity ratio of Raman absorption bands related to the anhydride (1857 cm^{-1}) and the styrene (1601 cm^{-1}). As such, the maximum percentages of MA to styrene ratio are 28% (SMA-4), 35% (SMA-1), 39% (SMA-5), and 52% (SMA-6), respectively. The maximum amounts of MA can be obtained after heating. These conditions correspond to the higher contact angle values, as the ring-closed MA is less hydrophilic than the ring-opened carboxylic acids.

The high sensitivity of contact angles to amount of MA suggests that the MA moieties are effectively located at the film surface, *i.e.*, at the outer surface of the spherical or fibrous structure. As such, the features are likely formed by self-organization of the hydrophobic styrene moieties pointing inwards of the spheres or fibers and the MA parts pointing outwards at the surface. The values for average surface roughness R_a were taken from 2 × 2 μm^2 AFM images. The more homogeneous coverage of spherical structures with smaller diameter (SMA-6) clearly provides the lowest roughness value. Otherwise, the changes in surface morphology upon heating result in some coarse structures with slightly higher roughness. This is most prominent for the films with lowest thermal stability. As a comparison, the average surface roughness of films with fibrous patterns was much higher: R_a = 86 nm (SMA-2, see AFM image in Figure 5b with mixed spherical and fibrous structures) and

120 nm (SMA-3, see AFM image in Figure 6c with fibrous structures). For the present polymer films, the differences in surface roughness do not directly correlate with the contact angle variations while the chemical composition seems to have a more direct influence. For other applications, it was found that the roughness affects the contact angles in a more direct way as estimated by the Wenzel model [56] for hydrophobic surfaces. In general, the roughness parameter increases the hydrophobicity on hydrophobic surfaces and augments the hydrophilicity on hydrophilic surfaces [57]. However, these trends could be attributed to the formation of hierarchical micro-to-nanoscale roughness structures that are not present in our case. Another reason could be the high structural variation and lack of regularity in the patterned films. In present situation, the water contact angles are primarily influenced by the chemical composition of the MA groups in the patterned films.

Table 4. Water contact angles (°) on different SMA copolymer films after deposition and heating at different temperatures (5 h).

SMA film	SMA-4		SMA-1		SMA-5		SMA-6	
	θ_{stat}	θ_a	θ_{stat}	θ_a	θ_{stat}	θ_a	θ_{stat}	θ_a
No heating	62	61	58	62	55	60	50	58
100 °C	60	58	50	68	48	64	49	62
120 °C	65	57	48	70	58	63	65	72
150 °C	55	50	68	75	58	65	55	65
180 °C	52	50	78	80	45	59	43	48
200 °C	48	49	58	68	40	59	32	46
220 °C	46	48	55	58	42	52	30	42
250 °C	42	48	38	46	35	43	22	35

Table 5. Amount of maleic anhydride (% MA) and average surface roughness (R_a) of the patterned films after deposition and heating at different temperatures (5 h).

SMA film	SMA-4		SMA-1		SMA-5		SMA-6	
	% MA [%]	R_a [nm]	% MA [%]	R_a [nm]	% MA [%]	R_a [nm]	% MA [%]	R_a [nm]
No heating	10	89	17	45	22	46	32	34
100 °C	12	105	14	52	20	50	32	33
120 °C	25	100	29	50	35	54	48	35
150 °C	25	130	34	60	38	62	52	36
180 °C	27	140	35	65	38	68	52	35
200 °C	28	122	35	76	39	73	52	36
220 °C	25	130	34	72	39	68	52	38
250 °C	25	126	33	85	37	80	48	37

4. Conclusions

This study describes the formation of patterned films from poly(styrene-*co*-maleic anhydride) or SMA, which are deposited from an acetone solution. The film morphologies illustrate the ability for self-assembly of molecular structures that were previously characterized as block copolymers with heterogeneous sequences of "styrene-rich" and "maleic anhydride-rich" segments.

Based on thermal analysis of original SMA pellets and cast films, the slightly higher glass transition temperatures for dried films indicate molecular arrangements. The presence of microscale structures in acetone is detected by dynamic light scattering and stability is confirmed by negative zeta-potential. The Raman spectroscopy of the acetone solutions mainly indicates formation of dimers with hydrogen bonds around C=O between the oxygen atom and the hydrogen atoms of a CH/CH_3-group. The anhydride groups in the SMA films have been partly converted by a ring-opening reaction, forming carboxylic groups that induce additional molecular interactions. After heating above 120 °C, the maleic anhydride moieties are restored.

The film patterns include microscale features formed by self-assembly of SMA copolymers: (i) polymer spheres form at molecular weights of 80,000 g/mol, with decreasing diameter as the amount of maleic anhydride increases, while (ii) fibrous structures form at molecular weights of 180,000 g/mol. Upon heating, the polymer spheres have high thermal stability and remain stable above the glass transition temperatures of the original SMA. After longer heating times, the patterned films re-assemble into short-fibrous ad long-fibrous polymer networks. This transition was first described qualitatively, but could be quantified by image processing of the micrographs indicating the relative quantities of each surface feature. Based on surface analysis after heating, the film reorganizes by dewetting effects and re-assembles into elementary particle sizes of around 100 nm diameter. The water contact angles on the patterned films are in the hydrophilic range and are primarily influenced by the amount of maleic anhydride moieties.

Acknowledgements

P.S. acknowledges the Robert Bosch Foundation for support in the Juniorprofessoren-program. G.S. would like to thank the Institute for the Promotion of Innovation by Science and Technology in Flanders for a funding program "SNAP" (contract grant IWT-080213). We thank H. van den Abbeele and D. Stanssens (Topchim N.V., Wommelgem, Belgium) for kindly providing materials.

Author Contributions

P.S. planned and performed experiments, processed data and wrote manuscript; G.S. made experimental plan and processed data.

Conflicts of Interest

The authors declare no conflict of interest.

References

1. Frank, C.W.; Rao, V.V.; Despotopoulou, M.M.; Pease, R.F.W.; Hinsberg, W.D.; Miller, R.D.; Rabolt, J.F. Structure in thin and ultrathin spin-cast polymer films. *Science* **1996**, *273*, 912–915.
2. Schäffer, E.; Harkema, S.; Roerdink, M.; Blossey, R.; Steiner, U. Thermomechanical lithography: Pattern replication using a temperature gradient driven instability. *Adv. Mater.* **2003**, *15*, 514–517.
3. Bang, J.; Kim, B.J.; Stein, G.E.; Russell, T.P.; Li, X.; Wang, J.; Kramer, E.J.; Hawker, C.J. Effect of humidity on the ordering of PEO-based copolymer thin films. *Macromolecules* **2007**, *40*, 7019–7025.
4. He, X.; Winkel, J.; Huck, W.T.S. Nanopatterning via pressure-induced instabilities in thin polymer films. *Adv. Mater.* **2009**, *25*, 2083–2087.
5. Amarandei, G.; Beltrame, P.; Clancy, I.; O'Dwyer, C.; Arshak, A.; Steiner, U.; Corcorana D.; Thieled, U. Pattern formation induced by an electric field in a polymer-air-polymer thin film system. *Soft Matter* **2012**, *8*, 6333–6349.
6. Wang, X.; Yin, J.; Wang, X. Self-structured surface patterns on epoxy-based azo polymer films induced by laser light irradiation. *Macromolecules* **2011**, *44*, 6856–6867.
7. Janes, D.W.; Katzenstein, J.M.; Shanmuganathan, K.; Ellison, C.J. Directing convection to pattern thin polymer films. *J. Polym. Sci. B Polym. Phys.* **2013**, *51*, 535–545.
8. Liu, D.; Wang, T.; Keddle, J.L. Protein nanopatterning on self-organized poly(styrene-*b*-isoprene) thin film templates. *Langmuir* **2009**, *25*, 4526–4534.
9. Yoo, P.J.; Suh, K.Y.; Park, S.Y.; Lee, H.H. Physical self-assembly of microstructures by anisotropic buckling. *Adv. Mater.* **2001**, *14*, 1383–1387.
10. Suh, K.Y.; Lee, H.H. Self-organized polymeric microstructures. *Adv. Mater.* **2002**, *14*, 346–351.
11. Reiter, G. Dewetting of thin polymer films. *Phys. Rev. Lett.* **1992**, *68*, 75–78.
12. Okerberg, B.C.; Berry, B.C.; Barvey, T.R.; Douglas, J.F.; Karim, A.; Soles, C.L. Competition between crystallization and dewetting fronts in thin polymer films. *Soft Matter* **2009**, *5*, 562–567.
13. Gavrilov, A.A.; Chertovich, A.V. Self-assembly in thin films during copolymerization on patterned surfaces. *Macromolecules* **2013**, *46*, 4684–4690.
14. Hue, J.C. Guided molecular self-assembly: A review of recent efforts. *Smart Mat. Struct.* **2003**, *12*, 264–271.
15. Boltau, M.; Walheim, S.; Mlynek, J.; Krausch, G.; Steiner, U. Surface-induced structure formation of polymer blends on patterned substrates. *Nature* **1998**, *391*, 877–879.
16. Zhang, L.; Zhang, H.L.; Bucknall, D.G. Self-assembly of polymer thin film on chemically patterned substrate. *Sol. State Phenom.* **2007**, *121–123*, 469–472.
17. Albert, J.N.L.; Epps, T.H. Self-assembly of block copolymer thin films. *Mater. Today* **2010**, *13*, 24–33.
18. Tanaka, K.; Takahara, A.; Kajiyama, T. Surface molecular aggregation structure and surface molecular motions of high-molecular-weight polystyrene/low-molecular-weight poly(methyl methacrylate) blend films. *Macromolecules* **1998**, *31*, 863–869.
19. Xue, L.; Han, Y. Pattern formation by dewetting of polymer thin film. *Prog. Polym. Sci.* **2011**, *36*, 269–293.

20. Xue, L.; Han, Y. Phase separation induced ordered patterns in thin polymer blend films. *Prog. Polym. Sci.* **2012**, *37*, 564–594.
21. Neto, C.; Jacobs, K.; Seemann, R.; Blossey, R.; Becker, J.; Grün, G. Correlated dewetting patterns in thin polystyrene films. *J. Phys. Condens. Matter* **2003**, *15*, S421.
22. Li, X.; Han,Y.; An, L. Inhibition of thin polystyrene film dewetting via phase separation. *Polymer* **2003**, *44*, 5833–5841.
23. Bowden, N.; Brittain, S.; Evans, G.; Hutchinson, J.W.; Whitesides, G.M. Spontaneous formation of ordered structures in thin films of metals supported on an elastomeric polymer. *Nature* **1998**, *393*, 146–149.
24. Ohzono, T.; Shimomura, M. Ordering of microwrinkle patterns by compressive strain. *Phys. Rev. B* **2004**, *69*, 132202.
25. Samyn, P.; Airoudj, A.; Mathew, A.P.; Roucoules, V.; Haidare, H.; Laborie, M.P. Metastable patterning of plasma nanocomposite films by incorporating cellulose nanowhiskers. *Langmuir* **2012**, 28, 1427–1438.
26. Walheim, S.; Böltau, M.; Mlynek, J.; Krausch, G.; Steiner, U. Structure formation via polymer demixing in spin-cast films. *Macromolecules* **1997**, *30*, 4995–5003.
27. Xie, R.; Karim, A.; Douglas, J.F.; Han, C.C.; Weiss, R.A. Spinodal dewetting of thin polymer films. *Phys. Rev. Lett.* **1998**, *81*, 1251–1254.
28. Jacobs, K.; Herminghaus, S.; Mecke, K.R. Thin liquid polymer films rupture via defects. *Langmuir* **1998**, *14*, 965–969.
29. Stamm, M.; Götzelmann, A.; Giessler, K.H.; Rauch, F. Organized structures in diblock copolymer films of polystyrene and poly-*para*-methylstyrene. *Prog. Colloid. Pol. Sci.* **1993**, *91*, 101–104.
30. Dutcher, J.R.; Dalnokio-Veressa, K.; Nickel, B.G.; Roth, C.B. Instabilities in thin polymer films: From pattern formation to rupture. *Macromol. Symp.* **2000**, *159*, 143–150.
31. Segalman, R.A. Patterning with block copolymer thin films. *Mater. Sci. Eng. R.* **2005**, *48*, 191–226.
32. Ramanathan, M.; Darling, S.B. Mesoscale morphologies in polymer thin films. *Prog. Polym. Sci.* **2011**, *36*, 793–812.
33. Hamley, I.W. Ordering in thin films of block copolymers: Fundamentals to potential applications. *Prog. Polym. Sci.* **2009**, *34*, 1161–1210.
34. Widawski, G.; Rawiso, M.; François, B. Self-organized honeycomb morphology of star-polymer polystyrene films. *Nature* **1994**, *369*, 387–389.
35. Hayakawa, T.; Kouketsu, T.; Kakimoto, M.; Yokoyama, H.; Horiuchi, S. Patterned surfaces in self-organized block copolymer films with hexagonally ordered microporous structures. *Macromol. Res.* **2006**, *14*, 52–58.
36. Hernandez-Guerrero, M.H.; Stenzel, M.H. Honeycomb structured polymer films via breath figures. *Polym. Chem.* **2012**, *3*, 563–577.
37. Zheng, Y.; Kubowaki, Y.; Kashiwagi, M.; Miyazaki, K. Process optimization of preparing honeycomb-patterned polystyrene films by breath figure method. *J. Mech. Sci. Technol*. **2011**, *25*, 33–36.
38. Yunus, S.; Delcorte, A.; Poleunis, C.; Bertrand, P.; Bolognesi, A.; Botta, C. A route to self-organized honeycomb microstructured polystyrene films and their chemical characterization by ToF-SIMS imaging. *Adv. Funct. Mater.* **2007**, *17*, 1079–1084.

39. Li, L.; Zhong, Y.; Gong, J.; Li, J.; Chen, C.; Zeng, B.; Ma, Z. Constructing robust 3-dimensionally conformal micropatterns: Vulcanization of honeycomb structured polymeric films. *Soft Matter* **2011**, *7*, 546–552.
40. Hahm, J.; Lopes, W.A.; Jaeger, H.M; Sibener, S.J. Defect evolution in ultrathin films of polystyrene-*block*-polymethylmethacrylate diblock copolymers observed by atomic force microscopy. *J. Chem. Phys.* **1998**, *109*, 10111–10114.
41. Knoll, A.; Horvat, A.; Lyakhova, K.S.; Krausch, G.; Sevink, G.J.A.; Zvelindovsky, A.V.; Magerle, R. Phase behavior in thin films of cylinder-forming block copolymers. *Phys. Rev. Lett.* **2002**, *89*, 035501:1–035501:4.
42. Mykhaylyk, T.A.; Collins, S.; Hamley, I.W.; Evans, S.D.; Henderson, J.R. Ordered structures and phase transitions in thin films of polystyrene/polyisoprene block copolymer and blends with the corresponding homopolymers. *J. Mater. Sci.* **2004**, *39*, 2249–2252.
43. Wang, M.; Zhu, X.; Wang, S.; Zhang, L. Surface pattern in thin poly(styrene-MA) films. *Polymer* **1999**, *40*, 7387–7396.
44. Wang, M.; Zhang, L. Hole pattern in polymer films and its template effect on the growth of gold particles. *Thin Solid Films* **2000**, *359*, 82–87.
45. Wang, S.X.; Wang, M.T.; Lei, Y.; Zhang, L.D. Mesoscopic self-assembling morphology of polymer based on emulsification. *Mater. Res. Bull.* **2000**, *35*, 1625–1630.
46. Martin-Garcia, B.; Velazquez, M.M. Block copolymer assisted self-assembly of nanoparticles into Langmuir-Blodgett films: Effect of polymer concentration. *Mater. Chem. Phys.* **2013**, *141*, 324–332.
47. Lopez-Diaz, D.; Velazquez, M.M. Evidence of glass transition in thin films of MA derivatives: Effect of the surfactant coadsorption. *Eur. Phys. J. E* **2008**, *26*, 417–425.
48. Martín-García, B.; Velazquez, M.M.; Pérez-Hernández, J.A.; Hernández-Toro, J. Langmuir and Langmuir-Blodgett films of a MA derivative: effect of subphase divalent cations. *Langmuir* **2010**, *26*, 14556–14562.
49. Song, S.; Li, L.; Zhang, J. Annealing improves tribological property of poly(octadecene-*alt*-MA) self-assembled film. *Appl. Surf. Sci.* **2011**, *257*, 10254–10260.
50. Schoukens, G.; Martins, J.; Samyn, P. Insights in the molecular structure of low- and high-molecular weight poly(styrene-MA) from vibrational and resonance spectroscopy. *Polymer* **2013**, *54*, 349–362.
51. Samyn, P.; Deconinck, M.; Schoukens, G.; Stanssens, D.; Vonck, L.; van den Abbeele, H. Synthesis and characterization of imidized poly(styrene-MA) organic nanoparticles in stable aqueous dispersion. *Polym. Adv. Technol.* **2012**, *23*, 311–325.
52. Lim, H.; Hoag, S.W. Plasticizer effects on physical-mechanical properties of solvent cast Soluplus® films. *AAPS Pharm. Sci. Tech.* **2013**, *14*, 903–910.
53. Lin, Y.; Tan, Y.Q.; Qiu, B.W.; Cheng, J.Q.; Wang, W.J.; Shangguan, Y.G.; Zheng, Q. Casting solvent effects on molecular dynamics of weak dynamic asymmetry polymer blend films via broadband dielectric spectroscopy. *J. Membr. Sci.* **2013**, *439*, 20–27.
54. Mirone, P.; Chiorboli, P. Infrared and Raman spectra and vibrational assignment of maleic anhydride. *Spectrochim. Acta* **1962**, *18*, 1425–1432.
55. Sasic, S.; Kuzmanovic, M. Raman spectroscopic study of acetone-phenol mixtures. *J. Raman Spectrosc.* **1998**, *29*, 593–599.

56. Wenzel, R.N. Surface roughness and contact angle. *J. Phys. Chem.* **1949**, *53*, 1466–1467.
57. Hobaek, T.C.; Leinan, K.G.; Leinaas, H.P.; Thaulow, C. Surface nanoengineering inspired by evolution. *BioNanoScience* **2011**, *1*, 63–77.